Bulletin of Engineering Geology and the Environment (2024) 83:150
https://doi.org/10.1007/s10064-024-03651-8

ORIGINAL PAPER

Combined effect of pore water pressure and axial stress level on the unloading mechanical properties of sandstone

Erping Zhao[1,2] · Han Zhang[1,2] · Guoliang Xiang[1,2] · Lehua Wang[1,2]

Received: 4 August 2022 / Accepted: 19 March 2024 / Published online: 1 April 2024

Abstract

For the stability evaluation of excavation engineering located in reservoirs, the combined effect of pore water pressure *P* and axial stress level *ASL* on the unloading mechanical properties of rocks is significant to study. The loading and unloading tests were performed on the sandstone under different *P*s and *ASL*s, and a novel method was proposed for evaluating the damage degree caused by the *P* and the unloading of confining stress during the unloading process of samples. The results showed that the strength and the unloaded amount of the sandstone decrease with the applied *ASL* and *P*. The area of cracks generated during the unloading increases with the *P* and *ASL*, indicating a higher damage degree under higher *P* and *ASL*. The development orientation of the crack is more inclined to the unloading direction under lower *ASL* and *P*, due to a larger unloading amount. The damage degree caused by the unloading of confining stress is higher under lower *ASL*, while the effect of *P* on the damage degree of samples is greater under higher *ASL*. It demonstrates that the developed method can be used for evaluating the damage degree of rocks during the unloading process, especially caused by the pore water pressure, while the traditional method cannot.

Keywords Unloading tests · Pore water pressure · Axial stress level · Unloading mechanical properties · Damage degree

Introduction

With the development of various engineering related to the excavation of rock mass, e.g., tunnels and excavation rock slopes, the unloading mechanical properties of rocks are significant to be studied for evaluating the stability of these excavation constructions. Li and Ha (1997) firstly pointed out the differences in mechanical properties of rocks in loading and unloading conditions, showing the significance of studying the unloading mechanical behaviors of rocks. It was found that the porosity, permeability, and cohesion of rock are smaller, while the friction angle is larger in the unloading condition compared with those in the loading condition (Wang et al. 2017, 2019; Zhang et al. 2020). Especially, in unloading condition, the deformation behavior of rock shows an obvious lateral expansion, the rock strength decreases with the increase of the unloading amount, and the failure pattern changes from compression-shear to tensile-shear (Liu et al. 2017; Wen et al. 2018; Zhang et al. 2021).

In recent years, some research focused on various influence factors on the unloading mechanical properties of rocks. For the applied initial confining stress before unloading, it was found that with the increase of the initial confining stress, the peak strength, lateral deformation, deformation modulus, and crack damage thresholds of rocks increase (Zhou et al. 2018; Liu et al. 2020), while the porosity and permeability decrease (Wang et al. 2020), and the failure mode changes from shear-tensile to tensile failure (Xu et al. 2019); furthermore, Zhao et al. (2020) and Chen et al. (2020a) proposed that as the initial confining stress increases, the increment of lateral strain of rock is larger than that of the axial strain. For the unloading rate, with the decrease of the unloading rate, the peak strength and the lateral deformation of rock increases (Deng et al. 2017; Li et al. 2017, 2019a), while the permeability decreases (Zhao et al. 2020), and a more obvious relaxation behavior of the rock sample is occurred (Yang et al. 2017), the failure mode changes from plastic to brittle pattern (Ren et al.

✉ Han Zhang
zhanghan@cug.edu.cn

1 Key Laboratory of Geological Hazards on Three Gorges Reservoir Area (China Three Gorges University), Ministry of Education, Yichang 443002, China

2 College of Civil Engineering & Architecture, China Three Gorges University, Yichang 443002, China

2021). For the unloading stress paths, Zhao et al. (2015) and Rong et al. (2020) pointed out that the strain growth rate and the peak strength were the largest under increasing axial stress during the unloading of confining stress, followed by a constant axial stress, then an unloading axial stress. For the water content, Wang et al. (2022) observed that the peak deviatoric stress of fractured rock decreases, and the elastic deformation is shortened while the yield deformation becomes more obvious during the unloading process. For the sample size, as the increase of height-to-width ratio of rock sample, it was found that the peak unloading strength of rock decreases, and the failure mode changes from tensile failure to shear failure (Li et al. 2017; Chen et al. 2020b). For the flaw inclination angle, Li et al. (2019b) pointed out the unloading strengths of the pre-flaw rock samples decrease with the increase of the flaw angle with the axial stress direction ranging from 0° to 90°. For the joint direction, Liu et al. (2016) showed that the peak deviatoric stress of mica-quartz schist is larger when the joint direction is parallel to the axial direction, compared to that perpendicular to the axial direction. In general, many research demonstrate the influence of initial confining stress, unloading rate, unloading stress paths, water content, sample size, flaw angle, and joint direction on the unloading mechanical properties of rocks are non-negligible.

Furthermore, some researches also pointed out the significance of the effect of pore water pressure and the axial stress level *ASL* on the unloading mechanical properties of rocks. Liu et al. (2020) suggested that the crack damage thresholds decrease with the pore water pressure, a more obvious volumetric expansion and yield failure occurred under a higher pore pressure. Wang et al. (2022) found the compressive strength and the elastic modulus of the fractured rock mass both have a reduction of 20% and 14% when the applied pore water pressure increases from 0.5 to 2.0 MPa, due to the hydraulic fracturing are easily formed between microcracks. Liu et al. (2017) found the peak strength of sandstone decrease with the applied axial stress level *ASL*, more specially, the friction angle has a reduction of 10%-15% with the applied *ASL* reducing 10%, and a more obvious brittle deformation and dilatation characteristics of the rock are observed under a lower *ASL*. Cong et al. (2020) suggested the peak bearing capacity of the rock is lower, and the fluctuations in strain energy is more significant under a lower *ASL*. Rong et al. (2021) observed that the fragmentation degree of the rock increase with the *ASL*, and more cracks generated by shear failure of bonds between particles. In conclusion, the previous researches indicated the influence of water pore pressure and the axial stress level on the unloading mechanical properties is great.

In the abovementioned researches, most of the studies focused on the unloading rate, stress path, etc. Some research also focused on the influence of water pore pressure or axial stress level. Few studies pay attention to the combined effect of the pore water pressure and the axial stress level on the unloading mechanical properties of rock mass. However, for the excavation engineering located in the reservoir with different depths, it is necessary to study the coupling effect of water and the initial axial stress on the unloading mechanical properties of rock mass, for providing scientific basis for the stability evaluation of the excavation engineering.

In this paper, the sandstone obtained from the Three Gorges Reservoir, China, was taken as the studied object. The triaxial tests were performed to provide a basis of the determination of axial stress level *ASL* for the unloading tests. The unloading mechanical properties and the internal structure damage of sandstone under different *ASL*s and pore water pressures were analyzed in detail by carrying out the trixial unloading tests and nuclear magnetic resonance scan. Furthermore, a novel method was proposed, based on the unloading strength and the strength parameters obtained by loading tests, for evaluating damage degree caused by the pore water pressure and the unloading of confining stress during the unloading process. Finally, the effect of pore water and *ASL* on the damage degree of sandstone during the unloading process was analyzed.

Materials and laboratory tests

Sandstone samples

The studied sandstone was obtained from the Three Gorges Reservoir, China. It is a sericite medium-grained quartz sandstone, composing of quartz, mica, and feldspar. The average value of dry density of the sandstone is 2.622 g/ cm^3 and its specific gravity is 2.729. 300 sandstone cylinder samples with a diameter of 50 mm and a height of 100 mm were prepared, and the wave velocities of the samples were measured by a sonic wave tester. The samples with similar wave velocities were selected for removing the effect of dispersion of samples on the test results (Fig. 1). Based on the selected value of wave velocity of samples, 64 samples were selected for the tests, 40 of them are necessary for the designed tests, and other 24 samples are spare samples for performing the repeated tests when the test results are unreasonable.

Triaxial loading and unloading tests

In order to study the influence of pore water pressure on the sandstone under different axial stress levels (*ASL*), loading and unloading tests were performed by a multifunctional rock triaxial test system (Fig. 2). The water pressure can be applied on the bottom of samples.

Fig. 1 Selected sandstone samples

Table 1 Triaxial loading tests

Sample ID	σ_3	*P*	Samples ID	σ_3	*P*
#5–1	5 MPa	0 MPa	#15–1	15 MPa	0 MPa
#5–2		0.3 MPa	#15–2		0.3 MPa
#5–3		0.6 MPa	#15–3		0.6 MPa
#5–4		0.9 MPa	#15–4		0.9 MPa
#5–5		1.2 MPa	#15–5		1.2 MPa
#10–1	10 MPa	0 MPa	#20–1	20 MPa	0 MPa
#10–2		0.3 MPa	#20–2		0.3 MPa
#10–3		0.6 MPa	#20–3		0.6 MPa
#10–4		0.9 MPa	#20–4		0.9 MPa
#10–5		1.2 MPa	#20–5		1.2 MPa

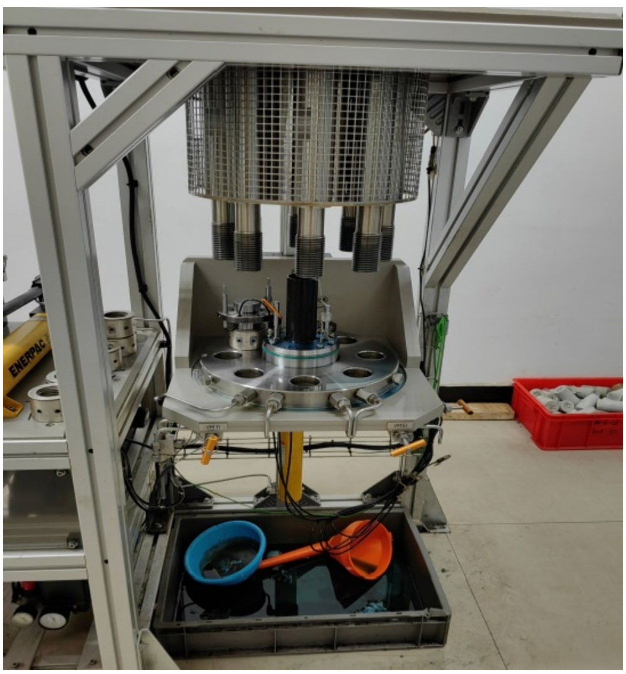

Fig. 2 Multifunctional rock triaxial test system

Table 2 Triaxial unloading tests

Sample ID	*ASL*	*P*	Sample ID	*ASL*	*P*
#30–1	30%	0 MPa	#70–1	70%	0 MPa
#30–2		0.3 MPa	#70–2		0.3 MPa
#30–3		0.6 MPa	#70–3		0.6 MPa
#30–4		0.9 MPa	#70–4		0.9 MPa
#30–5		1.2 MPa	#70–5		1.2 MPa
#50–1	50%	0 MPa	#90–1	90%	0 MPa
#50–2		0.3 MPa	#90–2		0.3 MPa
#50–3		0.6 MPa	#90–3		0.6 MPa
#50–4		0.9 MPa	#90–4		0.9 MPa
#50–5		1.2 MPa	#90–5		1.2 MPa

The different confining stresses σ_3 and water pressures *P*s were applied in the loading tests, as summarized in Table 1. The confining stress was firstly applied to a target value with a velocity of 0.1 MPa/min; then, the water pressure was applied on the bottom of the sample to a predicted value with a velocity of 0.01 MPa/min. After holding the water pressure stable at the target value for 30 min, the axial stress was gradually applied with 1.2 MPa/min until the sample was destroyed.

Different axial stress levels *ASL*s and pore water pressures *P*s were considered in the triaxial unloading tests, as listed in Table 2. The applied confining stress and water pressure are the same as those in the loading tests. Then, the axial stress was also applied with 1.2 MPa/min to reach a predicted value of $S = S_{max} \times ASL$, where S_{max} is the peak axial stress measured in the loading tests under the same confining stress and water pressure. Finally, the axial stress was unchanged and the confining stress was unloaded with a velocity of 0.1 MPa/min until the sample was destroyed.

Loading mechanical properties of sandstone

Deviatoric stress

The responses of deviatoric stress (σ_1-σ_3) versus axial strain ε_1 of sandstone samples under different pore water pressures are shown in Fig. 3. When the applied confining stress σ_3 is the same, the values of ε_1 of sandstone samples associated with the deviatoric stress reaching the peak values increase with the *P*. It indicates the failure pattern of the sandstone sample changes from brittle to plastic failure with the increase of *P*. It also shows a more remarkable plastic deformation of samples under higher *P*. The reason is the damage degree of the sample is higher during the

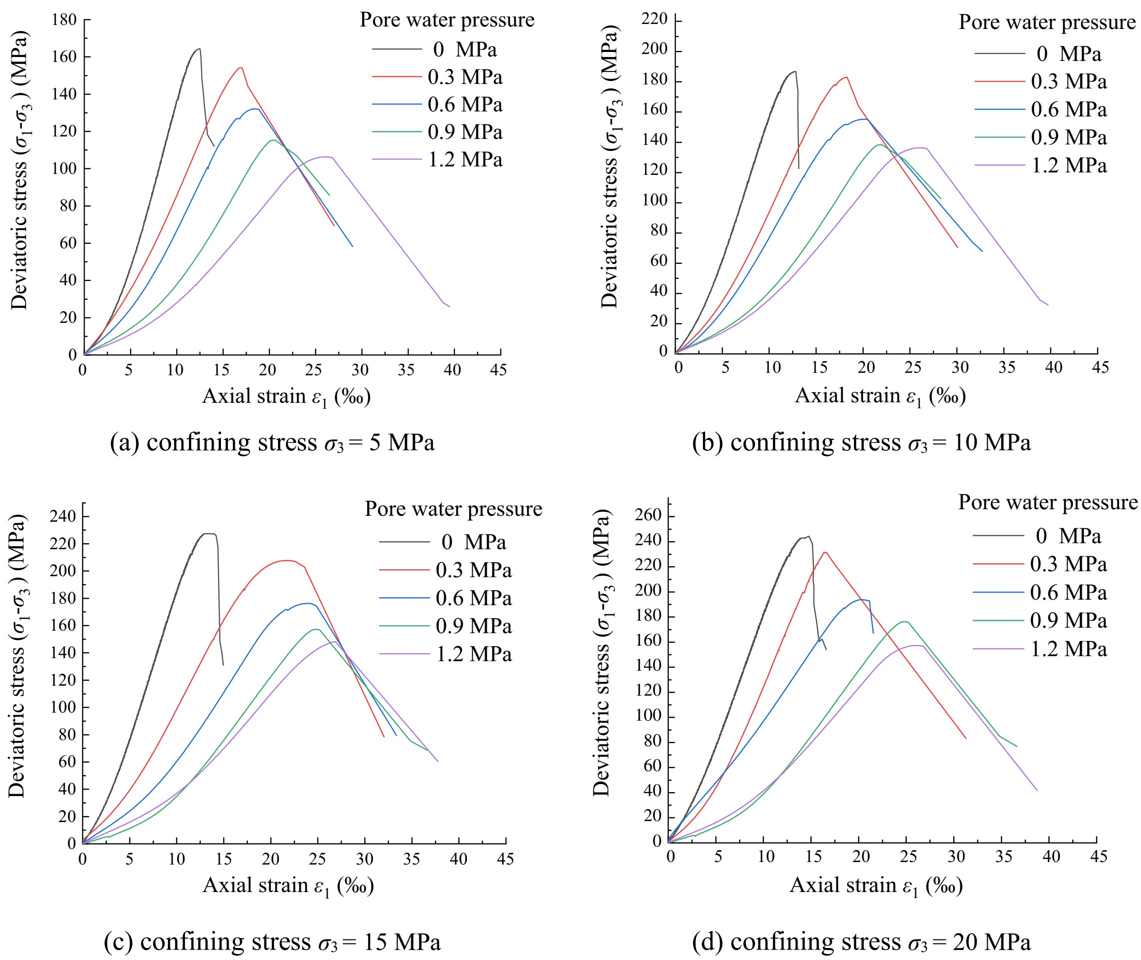

Fig. 3 a–d Deviatoric stress-axial strain curves under different pore water pressures and confining stresses

plastic deformation process under a higher applied P. When the cracks begin to generate in the rock during the plastic deformation, the applied water pressure leads to the water entering the crack and promoting the development of cracks, especially when the P is higher.

As illustrated in Fig. 4, the peak values of deviatoric stress of samples all decrease linearly with the P; however, different effect degrees of P on the peak stresses are observed in different confining stress conditions. The reduction magnitudes of peak stresses are larger under lower σ_3 (i.e., 5 MPa and 10 MPa), indicating the influence of P is greater when the confining stress is higher during the triaxial loading process.

Shear strength parameters

According to the Mohr–Coulomb strength criterion, the cohesion and friction angle of samples under different Ps are obtained (Fig. 5). With the increase of P, the cohesion and friction angle both decrease. The cohesion of samples

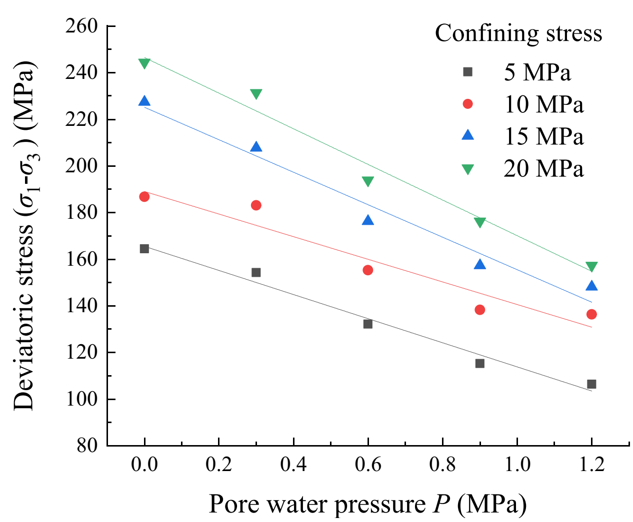

Fig. 4 Relationship of the peak deviatoric stress and pore water pressure under different confining stresses

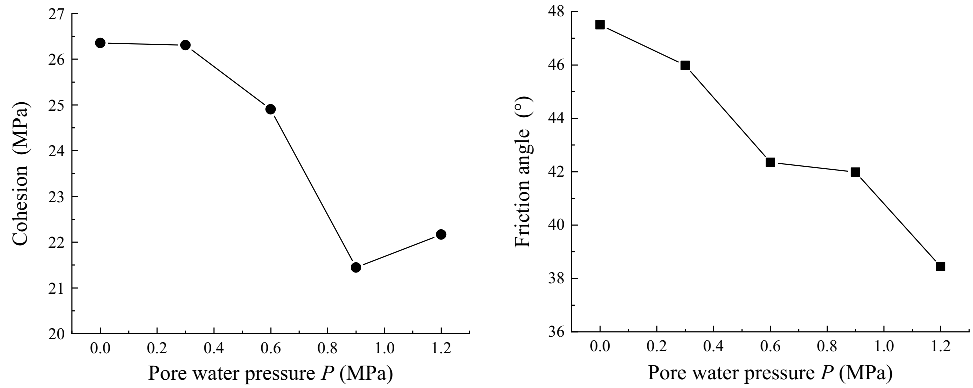

(a) cohesion (b) friction angle

Fig. 5 **a**, **b** Shear strength parameters of sandstone samples

decreases from 26.4 to 21.4 MPa with the increase of 1.2 MPa of the *P*, and the reduction ratio of cohesion reaches 18.9%. The friction angles of samples decrease linearly with the increase of *P*, 19.1% reduction of friction angle with increasing 1.2 MPa *P*. It demonstrates the increase in *P* greatly reduces the friction angle and cohesion of sandstone under loading condition, and the influence of *P* on the friction angle is the same as that on the cohesion.

Unloading mechanical properties under different water pressures

Deviatoric stress

The increment of deviatoric stress $F=\Delta(\sigma_1\text{-}\sigma_3)$ is used for describing the evolution of deviatoric stresses of samples during the unloading process. As shown in Fig. 6, when the *ASL* is 30%, the samples were destroyed until σ_3 was almost fully unloaded at lower *P* (i.e., 0 MPa and 0.3 MPa). And the same phenomenon is also observed on the sample without applying *P* when the *ASL* reaches 50%. However, the samples are destroyed during the unloading process for samples under larger *ASL* (i.e., 70% and 90%), and in the 30% and 50% *ASL* cases under higher *P*. It is because the crack generated during the loading process is less in the lower *ASL* and *P* conditions, making the rock difficult to destroy during the unloading of 5 MPa confining stress.

For the same *ASL*, the peak value of *F* decreases with the pore water pressure, and the deformation modulus of samples also has a reduction. The reduction of *F* caused by the increase of pore water pressure is larger under higher *ASL*. This is because the axial stress applied before the unloading is higher under higher *ASL*, leading to more cracks generated along the axial direction during the loading process. As such, when the water pressure is applied in the axial direction, the water can interact with the internal crack of rocks. For more cracks generated under higher *ASL*, the area of water pressure acting on the crack is larger, higher damage degree occurs. Therefore, the influence of pore water pressure is greater on the reduction of *F* in the higher *ASL* conditions.

When the *P* is the same, the peak value of *F* decreases rapidly with the *ASL* increasing from 30 to 90%, and the failure pattern changes from brittle to plastic failure pattern. The reduction of *F* caused by the increase of *ASL* is also larger under higher *P*. This phenomenon indicates that the damage of the rock internal structure caused by the pore water is greater under a higher *P*. It leads to a more obvious plastic deformation and a lower bearing capacity of sandstone in the higher *P* conditions.

Unloading amount

In order to analyze the influence of *P* and *ASL* on the unloading strength of samples, the unloading amount of confining stress *d* is introduced for evaluating the unloading strength as follows:

$$d = \sigma_3^0 - \sigma_3' \quad (1)$$

where the σ_3^0 and the σ_3' are the confining stress before the unloading and at failure, respectively. The larger the *d* is, the larger the unloading strength of the sample is.

As shown in Fig. 7, when the *ASL* is the same, the *d* values of samples decrease with the increasing *P*, and the reduction magnitudes are 10.49%, 20.66%, 45.84%, and 73.07% under different axial stress levels (i.e., 30% *ASL*, 50% *ASL*, 70% *ASL*, and 90% *ASL*), respectively. It indicates that the effect of *P* on the unloading strength is greater under a higher *ASL*. In the same *P* condition, the *d* has a reduction of 51.14%, 63.23%, 70.41%, 76.23%, and 85.30% with the *ASL* increasing from 30 to 90%. It shows the effect of *ASL* on the unloading strength under higher *P* is greater. It is because more cracks generated during the loading process when higher *ASL* and *P* were applied on the rock samples,

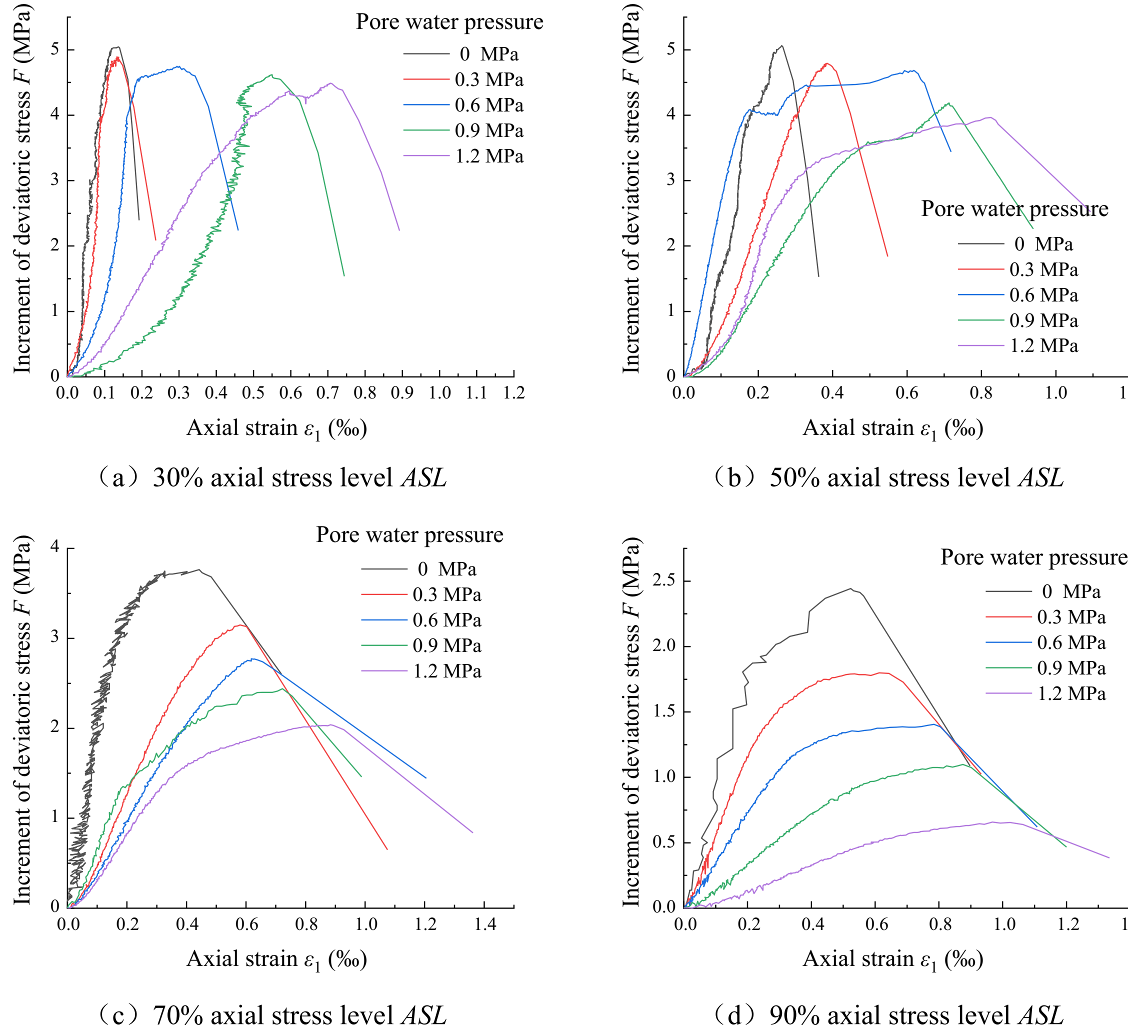

Fig. 6 **a–d** Deviatoric stress-axial strain curves under different pore water pressures and axial stress levels

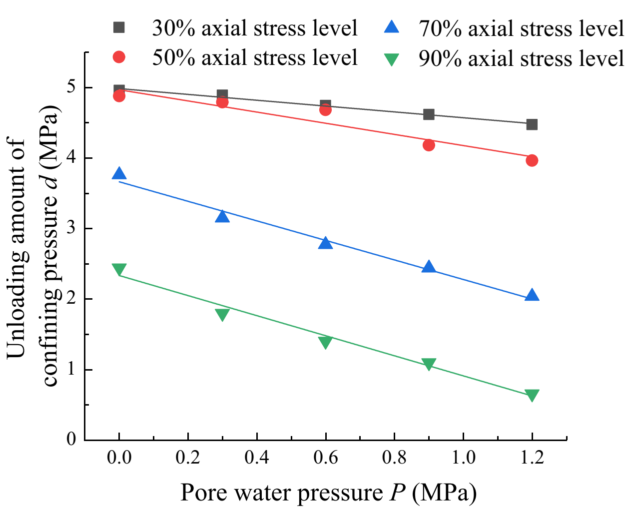

Fig. 7 Confining stress unloading amount under different axial stress levels and pore water pressures

giving rise to the damage during the unloading of confining stress is easier and the sample will destroy under a smaller unloading amount.

Moreover, the influence of P is greater than the *ASL* under lower *ASL*s (i.e., 30% and 50%), while the influences of *ASL* and P on the unloading strength of the samples are almost the same under higher *ASL*s (i.e., 70% and 90%). For the rock sample suffered lower axial stress before the unloading, e.g., the applied axial stress is less than 50% of the peak stress, the damage of rock internal structure is not obvious and the generated cracks are few. As such, the damage of rock sample has no obvious increment with the increase of *ASL* when the level is lower than 50%. It leads to the influence of *ASL* on the unloading amount is small when the *ASL* is less than 50%. However, when the applied axial stress before the unloading is higher than 50%, the rock sample experienced obvious internal structure damage; the deformation changes from elastic deformation to plastic deformation.

Therefore, the damage degree of rock sample will increase with the *ASL* when the level is higher than 50%. And the influence of increasing *ASL* on the unloading amounts of samples is great when the *ASL* is higher than 50%.

Strain confining compression compliance

In order to analyze the influence of the *ASL* and *P* on the axil deformation of samples during the unloading stage, the axial strain confining stress compliance $\Delta\varepsilon'$ is introduced for evaluating the effect degree, defined as the ratio of the axial strain increment $\Delta\varepsilon_1$ to the confining stress unloading increment $\Delta\sigma_3$ as follows (Qu et al. 2010; Huang et al. 2013):

$$\Delta\varepsilon' = \frac{\Delta\varepsilon_1}{\Delta\sigma_3} \tag{2}$$

The $\Delta\varepsilon'$ represents the increment of axial strain caused by the unloading of confining stress, the larger $\Delta\varepsilon'$ indicates a greater effect of the unloading on the axial deformation.

As shown in Fig. 8, the $\Delta\varepsilon'$ increases with the *P* and *ASL*, suggesting the effect of the unloading of confining stress is greater under higher *P* and *ASL*. For different axial stress levels (i.e., 30% *ASL*, 50% *ASL*, 70% *ASL*, and 90% *ASL*), the $\Delta\varepsilon'$ of samples has an increase of 116.40%, 134.73%, 141.87%, and 153.35% as *P* increasing from 0 to 1.2 MPa, respectively. It indicates the influence of pore water pressure on the axial deformaition of sample is greater under higher *ASL*. The $\Delta\varepsilon'$ of samples under different *P*s (i.e., 0 MPa, 0.3 MPa, 0.6 MPa, 0.9 MPa, 1.2 MPa) respectively has an increment of 161.10%, 169.89%, 215.40%, 222.37%, and 232.64% with *ASL* changing from 30 to 90%. It demonstrated that the greater effect of *ASL* on the axis deformation of samples in a higher *P* condition. Furthermore, the influence degree of *P* is smaller than that of *ASL* on the axis deformation of samples.

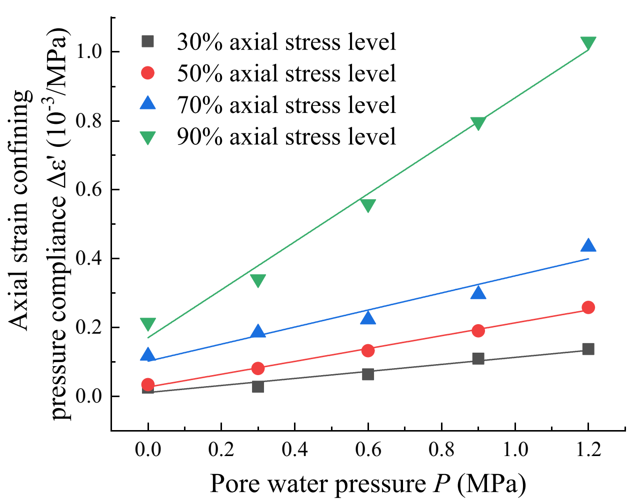

Fig. 8 Axial strain confining stress compliance of samples under different axial stress levels and pore water pressures

It is because the deterioration degree of the rock internal structure increases with *P* and *ASL*, leading to the development of more cracks. Therefore, a larger axial and lateral deformation occurred under higher applied *P* and *ASL*, characterized by a more obvious expansion phenomenon. The increase of *ASL* during the loading process will lead to the increase of crack area along the axial direction, especially under higher *ASL*. As such, more rock internal cracks can interact with the water, and the influence of pore water pressure will be more obvious under higher *ASL*.

Crack distribution characteristics

The rock samples were scanned by MacroMR12-150H-I Large aperture nuclear magnetic resonance (NMR) Imaging System (Core Analysis and Imager) in the Rock Laboratory of China Three Gorges University. As shown in Fig. 9, the rock sample was put in a cylindrical metal tube and scanned by using the NMImaging-V1 software. The scanned cross and longitudinal sections of rock samples are also exhibited in Fig. 9.

Figure 10 and Fig. 11 show the section images of rock samples obtained by the NMR scan, and the marking images of internal cracks under different *P*s and different *ASL*s. The white portion in the NMR image represents the water distribution in the samples in a saturated state and can be used to represent the internal cracks of samples.

As shown in the cross sections of samples under 1.2 MPa pore water pressure in Fig. 10. When the *ASL* is 30% and 50%, fewer cracks close to the edge of samples are observed in the samples, with a single crack and a small crack area. When the *ASL* reaches 70% and 90%, the cracks develop from the edge to the center of samples, characterized by a larger crack area, and the crack pattern changes from a single crack to "X" and "Y" cross cracks. It indicates that the damage degree of the sample is higher for a higher *ASL* as expected.

In the comparison of the longitudinal sections of the samples under different *ASL*s (Fig. 10), it can be also observed that the cracks are single cracks with a small area when the *ASL* is 30% and 50%. The cracks develop from the bottom to the center of the sample, along a direction at the angle of 61° and 75° from the horizontal direction, respectively. For the samples under higher *ASL*s, a larger crack area is found in the samples, and the crack pattern changes into an "X" type after the unloading. Moreover, the angle of the cracks increases to 78° and 84° for the samples under 70% and 90% *ASL*.

These phenomena show the crack area and the damage degree of rock samples increase with the *ASL*, and the crack development orientation is more inclined to the unloading

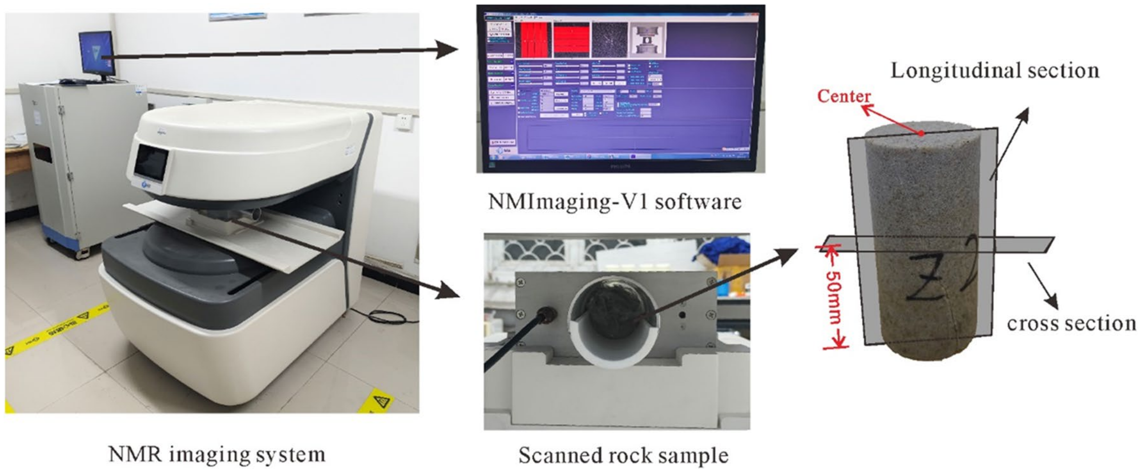

Fig. 9 The NMR imaging system and the cross and longitudinal sections of rock samples

Fig. 10 **a**–**h** NMR images of rock samples under 1.2 MPa pore water pressure

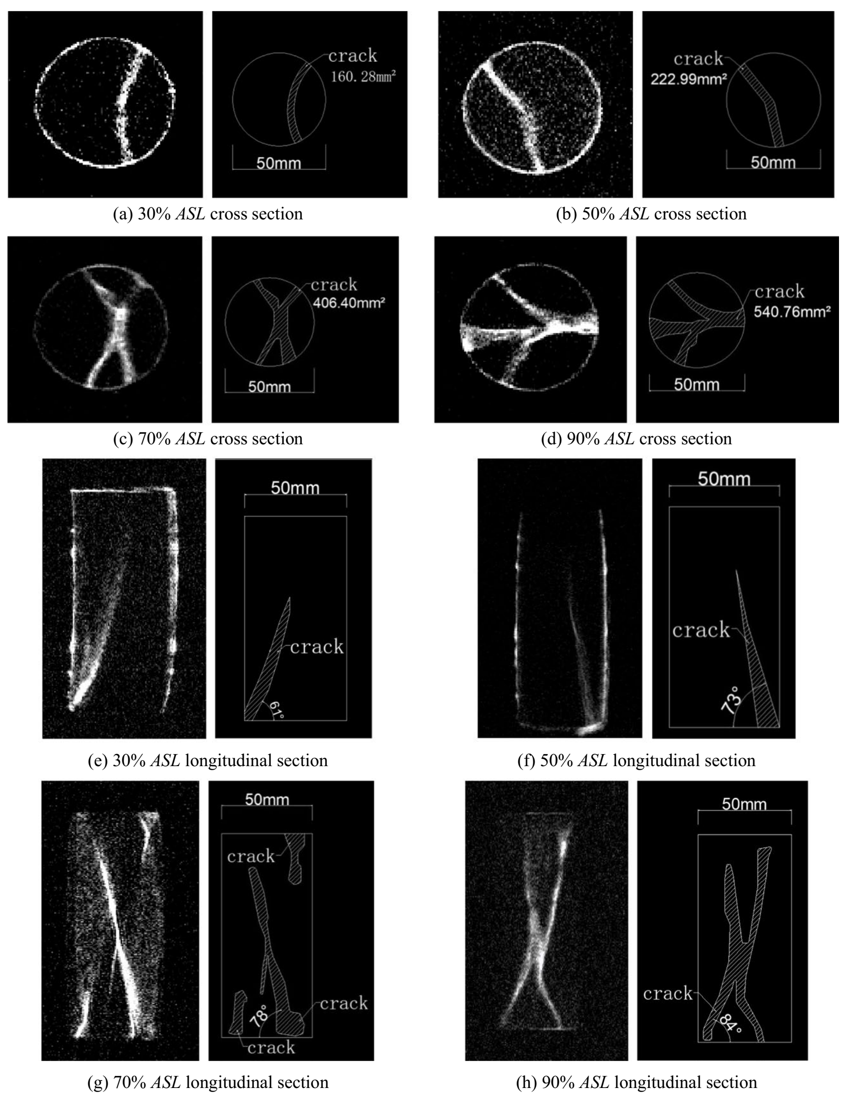

Fig. 11 **a**–**j** NMR images of rock samples under 90% axial stress level

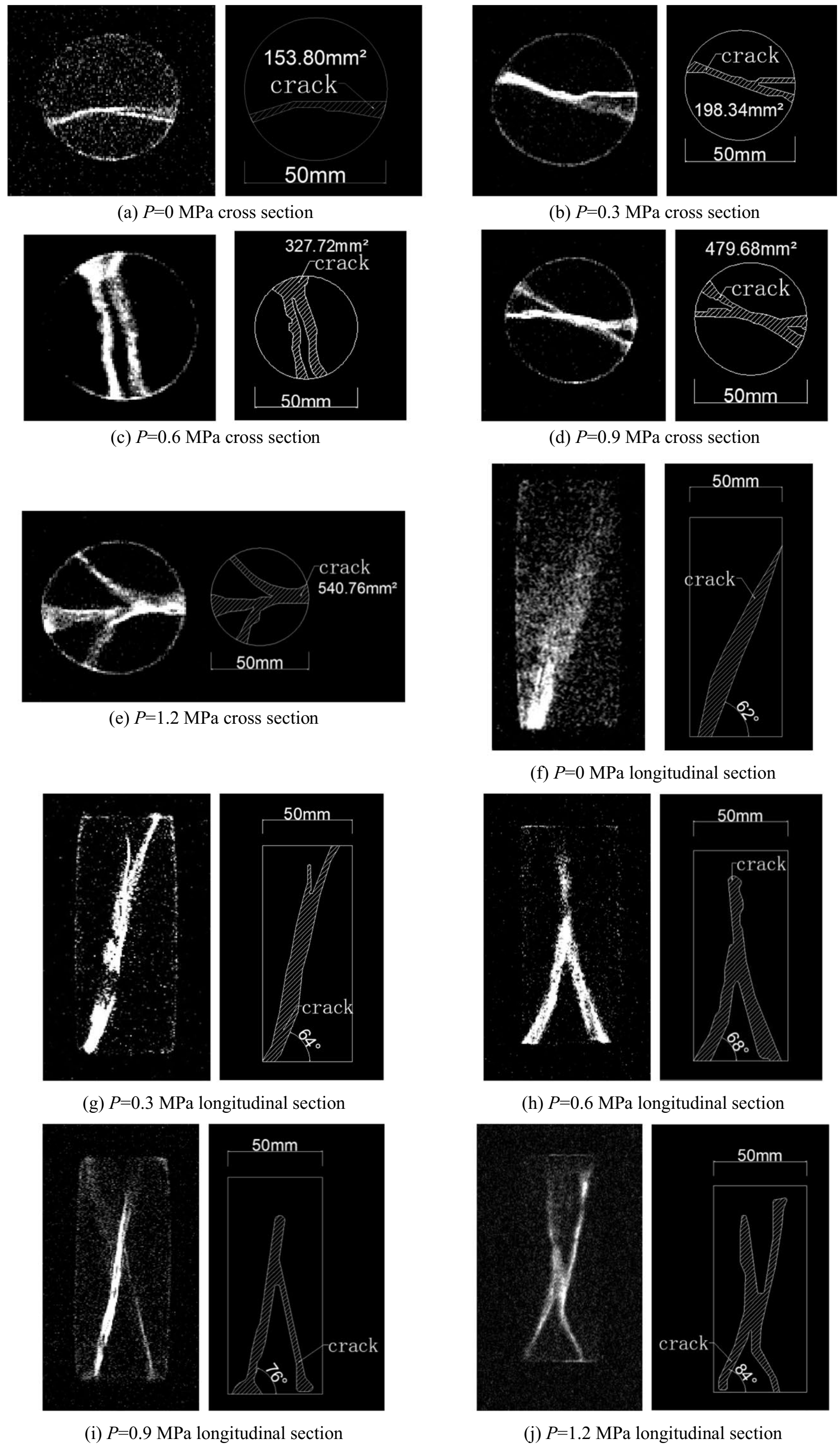

direction under lower *ASL* after the unloading of confining stress. With the increase of *ASL*, more cracks along the axial direction generated before the unloading of rocks. The rock samples will be destroyed under a smaller unloading amount and a shorter unloading process when the *ASL* is higher, while the samples suffer a longer unloading process under a lower *ASL*. As such, the cracks along the unloading direction mainly generated during the unloading process are more under the lower *ASL*. It leads to the crack direction of samples under lower *ASL* being more inclined to the unloading direction.

The effect of pore water pressure on the internal crack characteristics after unloading of samples was shown in Fig. 11. In relation to the sample under 90% *ASL*, it can be observed that the crack area also increases with the *P* from the cross sections of sample, and the crack pattern changes from a "Y" type to an "X" type. From the longitudinal sections of samples under different *P*s, the crack angle with the horizontal direction increases from 62° to 84° for the applied *P* increasing from 0 to 1.2 MPa. It indicates the increase of pore water pressure promotes the development of internal cracks, while restricting the lateral expansion phenomenon of samples. It is because the pore water pressure was applied along the axial direction, the higher water pressure will lead to more cracks generated along the axial direction. As such, the crack orientation is more inclined to the axial direction under higher applied *P*.

In addition, the increase magnitude of the crack area of samples with the increasing *P* is less than that with the increase of *ASL*. It suggests the effect of the *ASL* on the internal crack development is greater than that of the *P*. This is because the increase of 30% ASL can provide at least an additional 30 MPa axial stress. However, if the *ASL* is lower, the axial crack is few during the loading and unloading process, and the axial water pressure is difficult to interact with the internal cracks. As such, the 1.2 MPa water pressure only forces on the sample surface under lower *ASL*, the influence of only 1.2 MPa axial stress provided by water is smaller than the 30 MPa axial stress provided by the increase of *ASL*.

Effect of unloading and pore water pressure on the rock damage

In order to analyze damage effect during the unloading process of rock samples, Zhang et al. (2021) pointed out the traditional unloading damage parameter D_i as follows:

$$D_i = \frac{\sigma_{si} - \sigma_{xi}}{\sigma_{si}} \tag{3}$$

where σ_{xi} is the peak strength of the rock sample obtained in triaxial unloading condition, and σ_{si} is the peak strength of the same sample under the triaxial loading process.

In order to further study the effect of *P* and *ASL* on the damage degree of the sandstone samples during the unloading process, a novel method, based on the unloading strength and the strength parameters obtained by loading tests, is specially improved for evaluating the damage effect caused by *P* and *ASL* as follows:

$$D = \frac{(\sigma_1' - \sigma_1)}{\sigma_1'} \times 100 \tag{4}$$

$$\sigma_1' = \sigma_3 \times \tan^2\left(45^\circ + \frac{\varphi}{2}\right) + 2c \times \tan\left(45^\circ + \frac{\varphi}{2}\right) \tag{5}$$

where *D* is the developed unloading damage coefficient; σ_1 is the peak axial stress obtained in the unloading test; σ_1' is the theoretical peak strength calculated by the confining stress at the failure of unloading test, and the shear strength parameters obtained by the loading test; *c* and φ are the cohesion and friction angle obtained by the triaxial loading tests. The larger the *D* is, the more serious the damage to the rock sample during the unloading process.

For the traditional and the improved methods, the damage degrees during the unloading of the rock sample can be divided into two parts: (a) the damage degree caused by the unloading of confining stress, labeled as D_u; (b) the damage degree caused by the pore water pressure, labeled as D_p. The D_u can be directly obtained by the unloading tests without applying the pore water pressure. It is assumed that the effect of unloading is the same under the same *ASL*; then, the D_p of samples with an *ASL* and different *P*s can be calculated by $D_p = D - D_u$.

Combined with the experimental data obtained in this paper, the effect of unloading and the pore water pressure on the damage of samples are analyzed and compared by the use of the improved method and the traditional method proposed by Zhang et al. (2021).

Effect of unloading on the damage of sandstone

Figure 12 shows the damage degree caused by the unloading of confining stress D_u of samples during the unloading process obtained by the traditional and improved methods. The D_u values of samples decrease with the increase of *ASL*. It indicates the damage degree of the sample during the unloading is higher under smaller *ASL*, due to the sample suffering a larger unloading amount, as revealed from the internal crack distributions. The D_u reaches 65–70% when the applied *ASL* is 30%, and the D_u reduces to only 3–10%

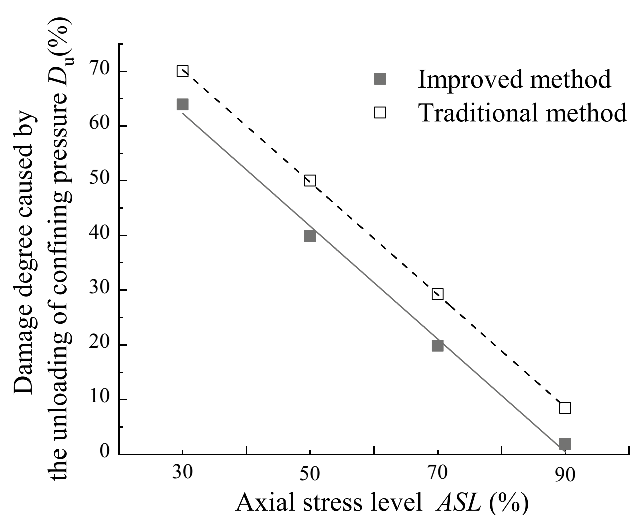

Fig. 12 Damage degree of samples caused by the unloading of confining stress

for the 90% *ASL* case. It demonstrates the influence of *ASL* is great for the damage of samples caused by the unloading.

In comparison to the results obtained by the traditional method, the D_u obtained by the improved method is lower. However, the differences in D_u values of samples calculated by the two methods under the same *ASL* are only 5–7%, suggesting they can be both used for evaluating the damage degree of rock caused by the unloading of confining stress.

Effect of pore water pressure on the damage of sandstone

To study the effect of *P* on the damage degree of the sandstone, the damage degree caused by the pore water pressure D_p of samples under different *ASL*s and *P*s, by removing the portion caused by the unloading, are shown in Fig. 13. By adopting the improved method, the D_p of samples increases linearly with the *P* under all *ASL* conditions. It indicates that the increase of *P* promotes the damage of samples and leads to a higher damage degree during the unloading process. This is because the applied pore water pressure acts on the generated cracks caused by the unloading and accelerates their development. This phenomenon is the same as that observed in the NMR images under different *P*s, while it is different from the results obtained by the traditional method, demonstrating the proposed improved methods can be used for evaluating the damage caused by the *P* while the traditional one cannot.

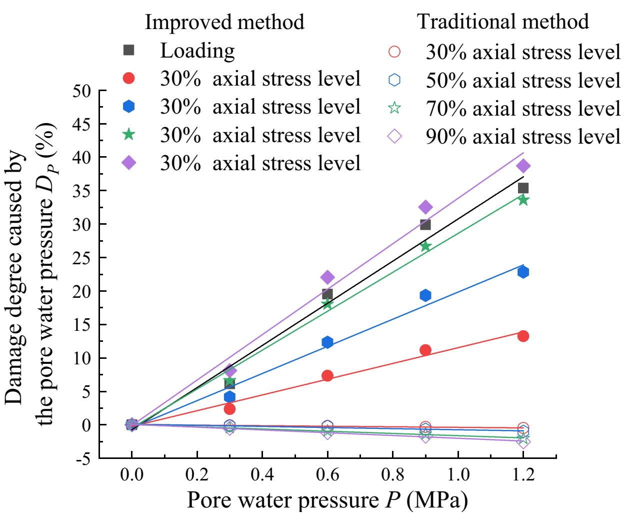

Fig. 13 Effect degree of pore water pressure on the damage of samples

The increment magnitude of D_p with the *P* is larger for a higher *ASL* case, indicating the *P* has a more significant effect on the damage of the sample under a higher *ASL*. And the damage degrees caused by the *P* of samples under unloading with higher *ASL*s (i.e., 70% and 90%) are the same as those under triaxial loading conditions. It is because the cracks mainly develop along the direction of axial stress for the sample under loading condition (Fig. 14a) and unloading condition with higher *ASL* (Fig. 14c), same as the description in the NMR images. While the internal cracks direction of the sample under lower *ASL* is more inclined to the direction of confining stress (Fig. 14b), due to a more significant lateral expansion deformation caused by a larger unloading amount. The pore water pressure applied from the bottom of the samples has a greater effect on the development of cracks along the axial stress direction than the confining stress direction, leading to more significant damage for samples in loading conditions and unloading conditions with higher *ASL*s.

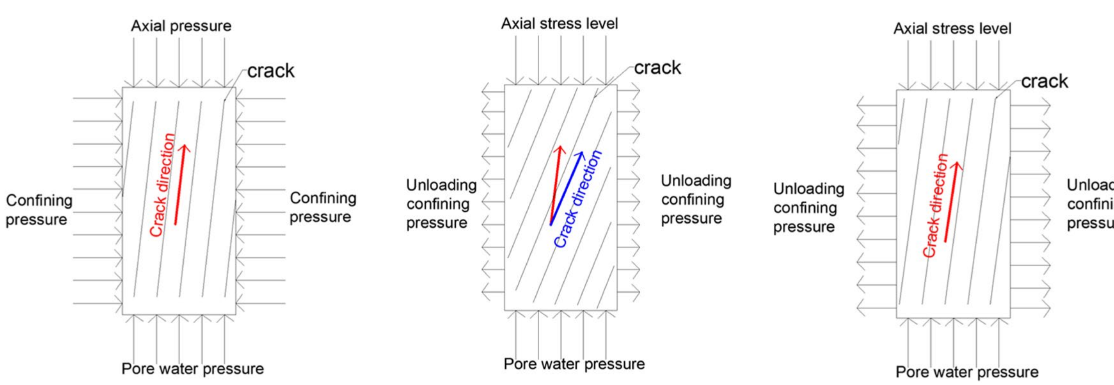

(a) loading (b) unloading under lower *ASL*s (c) unloading under higher *ASL*s

Fig. 14 **a**–**c** Schematic diagram of internal damage during loading and unloading (the red arrows represent the crack direction of samples in loading condition and unloading condition with higher *ASL*; the blue arrow represents the crack direction of samples in unloading condition with lower *ASL*)

Damage degree of sandstone during unloading process

As shown in Fig. 15, the damage degrees of sample obtained by the improved method is lower than those obtained by the traditional method under lower *P*, while it is inverse under higher *P*. It is because the traditional method cannot be used for evaluating the effect of *P* on the damage of samples accurately. However, the improved method can overcome this disadvantage, for accurately evaluating the damage degree of samples, not only caused by the unloading of stress, but also caused by the pore water pressure.

Under the combined influence of *ASL* and *P*, the damage degree of sandstone increases with the *ASL* and *P*, and the increment magnitude of *D* with the *ASL* is larger than that with the *P*. It indicates the increase of *ASL* and *P* both promote the damage of sandstone during the unloading process, and the influence of *ASL* is greater than the *P*. This is because the damage of samples during the unloading process is mainly caused by the unloading of confining stress.

Conclusions

In this paper, triaxial loading and unloading tests were carried out for studying the combined influence of pore water pressures and axial stress levels on the unloading mechanical properties and internal crack development of sandstone. A novel method was improved on the basis of the unloading strength and the strength parameters obtained by loading tests, for evaluating damage degree caused by the pore water pressure and the unloading of confining stress during the unloading process. The following conclusions were drawn:

1) During the loading process, with the increase of the *P*, the peak strength and the shear strength parameters of sandstone decreases, and the failure mode changes from brittle failure to plastic failure. The effect degree of pore water pressure on the φ is the same as that on the *c* of sandstone.
2) During the unloading process, with the increase of the applied *ASL* and *P*, the peak deviatoric stress and the unloaded amount of the sandstone decrease, while the axial strain confining stress compliance increases. It indicates that the higher applied *P* and *ASL* promotes the damage of samples, leading to a weakened bearing capacity and a larger deformation of samples.
3) The increase of *P* and *ASL* both promote the development of internal cracks during the unloading process, and the effect of *ASL* is greater. Moreover, the development orientation of the crack is more inclined to the unloading direction for a sample under lower *ASL* and *P*, showing a more significant lateral expansion of samples.
4) The damage degree of samples caused by the unloading of confining stress is higher under smaller *ASL*. The damage degree of samples caused by the pore water pressure increases with the *P*, and the effect of *P* is greater under higher *ASL*s. The increase of *ASL* and *P* both promote the damage of sandstone during the unloading process, mainly caused by the unloading of confining stress. It demonstrates that the developed method can be used for evaluating the damage degree of rocks during the unloading, especially for the damage caused by the pore water pressure, while the traditional method cannot.

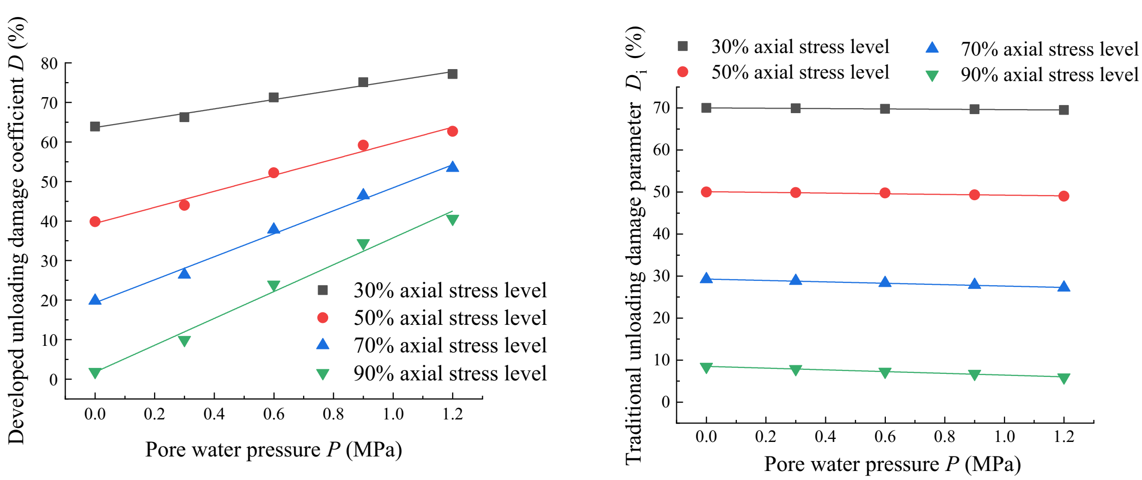

(a) Improved method (b) Traditional method

Fig. 15 **a**, **b** The damage degree of samples during the unloading process under different axial stress levels and pore water pressures

Notation list *ASL*: Axial stress level; *P*: Pore water pressure; σ_3: Confining stress; σ_1: Axial stress; ε_1: Axial strain; *F*: Increment of deviatoric stress; *d*: Unloading amount of confining stress; $\Delta\varepsilon\prime$: Axial strain confining stress compliance; D_i: Traditional unloading damage parameter; *D*: Developed unloading damage coefficient; D_u: Damage degree caused by the unloading of confining stress; D_p: Damage degree caused by the pore water pressure

Funding This study is funded by the High Speed Rail Joint Fund (No. U2034203), National Natural Science Foundation of China (No. 42207218), National Natural Science Foundation of China (No. U23A2045), Natural Science Foundation of Hubei Province (No. 2020CFA049), Guangdong Basic and Applied Basic Research Foundation (2021A1515110723).

References

Chen C, Liu LP, Cong Y (2020a) Experimental investigation on deformation and strength behavior of marble with the complex loading-unloading stress path. Math Probl Eng 2018:8294390

Chen ZH, Huang LQ, Li XB et al (2020b) Influences of the height to diameter ratio on the failure characteristics of marble under unloading conditions. Int J Geomech 9:04020148

Cong Y, Wang ZQ, Zheng YR et al (2020) Effect of unloading stress levels on macro and microfracture mechanisms in brittle rocks. Int J Geomech 20(6):04020066

Deng, H.F., Wang, Z., Li, J.L. (2017) Effect of unloading rate and pore water pressure on mechanical properties of sandstone. Chinese J. Chinese J Rock Mecha Eng 39(11): 1977–1983. (in Chinese)

Huang, X., Liu, Q.S., Lu, X.L. et al. (2013) For deep soft ground TBM excavation surrounding rock mechanics behavior experimental study (II): unloading rate effect and deformation mechanism. Chinese J. Chinese J Rock Mech Eng 36(6): 1–12. (in Chinese)

Li JL, Ha QG, (1997) Three-dimensional numerical simulation of macroscopic mechanical parameters of the Three Gorges unloading rock mass. Chinese J. J Wuhan University of Hydraulic and Electric Power (Yichang) 1997(03): 1–6. (in Chinese)

Li JZ, Lin F, Liu HF et al (2019a) Triaxial experimental study on changes in the mechanical properties of rocks under different rates of confining pressures unloading. Soil Mech Found Eng 56(4):246–252

Li XB, Chen ZH, Weng L (2019b) Unloading responses of pre-flawed rock specimens under different unloading rates. Trans Nonferrous Metals Soc China 29:1516–1526

Li, X.B., Chen, Z.H., Cao, W.Z. (2017) Time-effect properties and mechanisms of marble failure under different unloading rates. Chinese J. Chinese Journal of Geotechnical Engineering 39(9): 1565–1574. (in Chinese)

Liu SL, Zhu QZ, Shao JF (2020) Deformation and mechanical properties of rock: effect of hydromechanical coupling under unloading conditions. Bull Eng Geol Env 79:5517–5534

Liu, Z.Y., Xiao, M.L., Zhuo, L. et al. (2016) Study on mechanical properties of quartz mica schist with unloading and unloading constitutive. Chinese J. Chinese Journal of Geotechnical Engineering 38 (S2): 85–91. (in Chinese)

Liu, X.R., Liu, J., Li, D.L. et al. (2017) Mechanical properties and unloading constitutive model of sandstone under different water pressures and initial unloading levels. Chinese J. Chinese Journal of Coal Society 42(10): 2592–2600. (in Chinese)

Qu, S.L., Feng, X.T., Zhang, C.Q. et al. 2010. Different unloading confining pressure rate of deep buried marble unloading mechanical properties test and research. Chinese J. Chinese J Rock Mech Eng 29(9): 1807 - 1817. (in Chinese)

Ren JX, Yun MC, Zhang K et al (2021) Mechanical properties of fine grained granite under different unloading confining pressure rates. Chinese J Science Technology and Engineering 21(29):12672–12678 (in Chinese)

Rong HY, Li GC, Zhao GG et al (2020) Experiment on true triaxial unloading characteristics of deep rock under different stress paths. Chinese J Journal of Coal Society 45(09):3140–3149 (in Chinese)

Rong HY, Li GC, Xu JH et al (2021) Particle flow simulation of failure characteristics of deep rock influenced by sample height-to-width ratios and initial stress level under true-triaxial unloading. Geofluids 2021:6631744

Wang HL, Xu WY, Cai M et al (2017) Gas permeability and porosity evolution of a porous sandstone under repeated loading and unloading conditions. Rock Mech Rock Eng 50:2017–2083

Wang JJ, Liu MN, Jian FX et al (2019) Mechanical behaviors of a sandstone and mudstone under loading and unloading conditions. Environ Earth Sci 78:30

Wang RB, Xu B, Wan Y et al (2020) Characteristics of unloading damage and permeability evolution of sandstone under hydromechanical coupling. Eur J Environ Civ Eng 4:1–10

Wang ML, Li XS, Yang S et al (2022) Research on deformation and fracture characteristics of the fractured rock mass under coupling of heavy rainfall infiltration and mining unloading. Front Earth Sci 2021:792038

Wen, T., Tang, H.M., Fan, Z.Q. et al. 2018. Mechanical properties of rock loading and unloading in Badong Formation and unloading constitutive model. Chinese J. J China University of Mining and Technology 47(04): 768–779. (in Chinese)

Xu H, Feng TX, Yang CX et al (2019) Influence of initial stresses and unloading rates on the deformation and failure mechanism of Jinping marble under true triaxial compression. Int J Rock Mech Min Sci 117:90–104

Yang HQ, Liu JF, Zhou XP (2017) Effects of the Loading and unloading conditions on the stress relaxation behavior of pre-cracked granite. Rock Mech Rock Eng 50:1157–1169

Zhang HB, Wang LH, Li JL et al (2021) Mechanical properties of sandstones under initial unloading damage. Adv in Civil Eng 2021:6615846

Zhang Y, Yang YJ, Ma DP (2020) Mechanical characteristics of coal samples under triaxial unloading pressure with different test paths. Shock Vib 2020:8870821

Zhao HG, Liu C, Huang G (2020) Dilatancy behaviour and permeability evolution of sandstone subjected to initial confining pressures and unloading rates. R Soc Open Sci 8:201792

Zhao, G.Y., Dai, B., Dong, L.J., et al. (2015) Study on mechanical properties and strength criteria of rock triaxial unloading under different stress paths. Chinese J. Rock Soil Mech 36(11):3121–3127+3149. (in Chinese)

Zhou KP, Liu TY, Hu ZX (2018) Exploration of damage evolution in marble due to lateral unloading using nuclear magnetic resonance. Eng Geol 244:75–85